Mixing in Stratified Lakes and Reservoirs

Damien Bouffard and Alfred Wüest

Abstract Aquatic physics in inland water is a crucial subject for studying aquatic ecosystems. Transport and mixing are of tremendous importance for the pace at which chemical and biological processes develop. Recent observations allow to distinguish mixing and transport processes in stratified lakes and reservoirs. The surface and bottom boundary layer are turbulent while the lake interior remains comparatively quiescent.

1 Introduction

Lakes and reservoirs receive thermal energy mainly through the lake surface. The net heat flux H is the sum of all heat flux contributions, including the shortwave absorption (positive), the longwave absorption (positive), the longwave emission (negative), the heat flux by evaporation and condensation, the heat convection (free and forced), and the heat flux caused by throughflow. The latter three components can have either sign. If H is negative, the water body loses heat (typically in autumn and winter in the Northern hemisphere) and if positive, thermal energy is stored in the water body (typically spring and summer). Most of the heat is stored in the very top layers and some of it is slowly transported into deeper parts by vertical turbulence. In lakes, reservoirs, and estuaries this vertical transport is slow, whereas in rivers the heat is quickly homogenized. In lakes, a change in the heat balance may have most effects on surface water temperatures and less effects on the much larger deep-water volume.

D. Bouffard (✉) · A. Wüest
Swiss Federal Institute of Aquatic Science and Technology,
EAWAG, Kastanienbaum, Switzerland
e-mail: Damien.bouffard@eawag.ch

A. Wüest
Physics of Aquatic Systems Laboratory, Ecole Polytechnique
Federale de Lausanne, EPFL, Lausanne, Switzerland
e-mail: alfred.wueest@eawag.ch

H.J.H. Clercx and G.J.F. Van Heijst (eds.), *Mixing and Dispersion in Flows Dominated by Rotation and Buoyancy*, CISM International Centre for Mechanical Sciences 580,
https://doi.org/10.1007/978-3-319-66887-1_3

The density ρ of natural waters depends on temperature and pressure as well as on dissolved and suspended constituents (relevant are salts, gases, and particles) in the water. Under natural conditions, the water column is always stratified to some extent, mostly by temperature gradients, often by salinity gradients (especially in oceans and deep lakes) and almost always by both (oceans). In the following, we only consider the temperature dependences.

Accumulation of thermal energy in the near-surface layers leads to a thermal stratification separating a warm upper layer from a colder lower layer with a thermal barrier called thermocline. The location of the thermocline varies over the season, depending on the competition between heat and momentum (wind) forcing. Stratification has many ecological consequences. During the stratified period, the thermocline prevents vertical fluxes, isolating the hypolimnion from gas exchanges with the atmosphere. Without an influx of oxygen, the hypolimnion can become depleted of oxygen during the summer stratified period due to oxygen use by bacterial decomposition of organic matter mostly in the sediment.

The annual cycle of lake water temperatures in temperate lakes is typically as follows. In spring, an overturn, a complete vertical mixing, of the lake water body happens. Another overturn happens in autumn, when the surface waters have been cooled so that they are heavier than the deep waters. Overturns and deep mixing events are important to the vertical exchange and renewal of deep waters, for instance for deep oxygen enrichment. In summer most of the lakes in the temperate climatic zone are stratified. The warm surface layer extending down to 5–20 m is called the epilimnion. Below is the thermocline (also called metalimnion), where the water temperature decreases rapidly over a few meters. Below is a colder layer called the hypolimnion. Besides the seasonal temperature and stratification variation, diurnal thermal variations are also present in lakes and reservoirs. This happens especially during calm cloudless summer days and nights. The solar radiation heats up the surface waters increasing day-time stratification with some extra layers in the epilimnion. Nocturnal cooling of air leads to strong sensible heat loss from the lake surface, which is also emitting heat by long-wave radiation. The cooled waters sink down and cause vertical mixing and this leads to the well mixedness of the epilimnion.

2 Surface and Bottom Boundary Layers in Lakes

2.1 The Role of Boundary Layers in Natural Waters

In stratified waters (ocean, lakes, reservoirs, wetlands) the boundary layers are the most dynamic zones. In the surface boundary layer (SBL) light and nutrients enable photosynthesis by phytoplankton, which provides the basis of the food web for zooplankton and fish. Also physical, biological, geochemical, and photochemical processes undergo the strongest dynamics here owing to exchange with the adjacent atmosphere, light intensity and heat fluxes. Hence, for understanding the ecologically

most relevant phenomena, the atmosphere-water relationship is crucial. Depending on the properties of the atmosphere (wind, temperature, humidity, etc.) and the water surface (waves, surfactants, etc.) the air-water interface creates a bottleneck for the exchange of the physical quantities such as heat and matter (gases, vapour, aerosols; in both directions) or momentum and mechanical energy (from air to water). These exchanges of physical and chemical properties are driven by wind and heat flux induced turbulence on both sides of the interface, see the schematics in Figs. 1 and 2.

Also the bottom boundary layer (BBL) is an active zone, as there the currents approach zero and therefore shear zones develop with much higher level of turbulence than in the interior of the stratified water body, see Fig. 1. The BBL is also important for the exchange of oxidants and reduced substance with the sediment and the resuspension and net sedimentation of particulate substances. Especially important are fluxes of oxygen for the decomposition of organic matter in the sediment.

First we discuss the SBL, which is more complex due to the free surface (velocity not zero at the surface) and the presence and breaking of waves and the subsequent entrainment of air into the water.

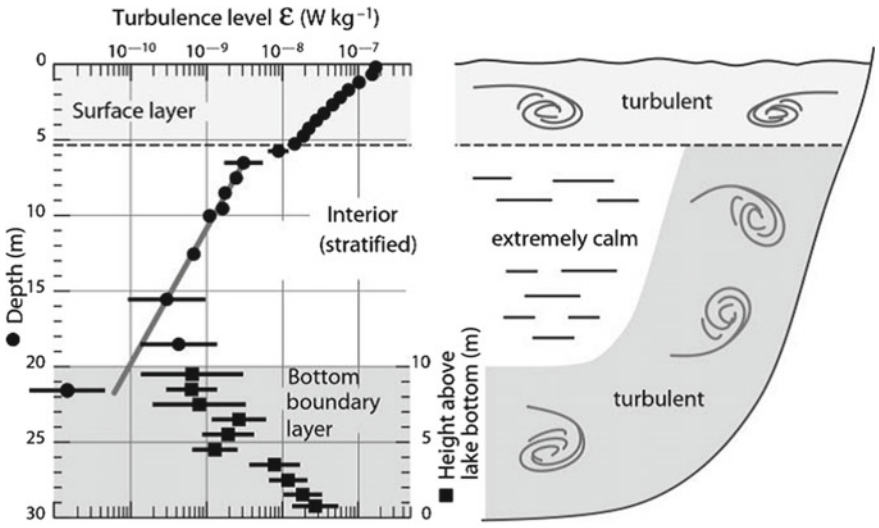

Fig. 1 Level of turbulence in a medium-sized lake, expressed by dissipation ε of turbulent kinetic energy, as a function of depth (*circles*) and as a function of height above the *bottom* (*squares*). The plot motivates characterizing the three distinctly different water bodies separately: the energetic SBL, the slightly less turbulent bottom boundary layer, and the strongly stratified and almost laminar interior. Courtesy of Wüest and Lorke (2003)

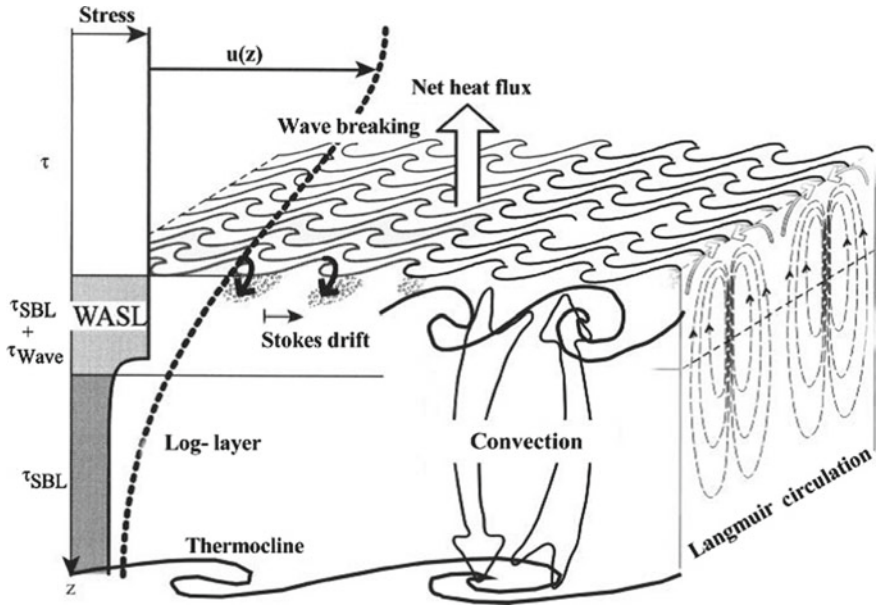

Fig. 2 Schematic overview of the surface boundary processes, the shear stress, and the associated vertical structure of the SBL. Stokes drift = net horizontal flow due to the effect of the inhomogeneous orbiting of wave-induced currents. Convection = vertical up/down plumes due to surface cooling. Log-layer = turbulent BL, where logarithmic $u(z)$ profiles applies. Langmuir circulation = second-order flow cells perpendicular to the driving wind. Courtesy of Wüest and Lorke (2003)

2.2 The Turbulent Kinetic Energy Balance

We derive the equation for the turbulent kinetic energy (TKE) from the simplified Navier Stokes equation,

$$\frac{\partial U_i}{\partial t} + U_j \frac{\partial U_i}{\partial x_j} = -\delta_{i3} g - \frac{1}{\rho} \frac{\partial p}{\partial x_i} + \nu \frac{\partial^2 U_i}{\partial x_j^2}$$

$$(I) + (II) = (III) + (IV) + (V)$$

(I = acceleration of velocity i; II = advection; III = gravity (3^{rd} (z) component only); IV = pressure force and V = friction by viscosity). Here, and later on, the Einstein summation convention is adopted which means that a repeated index (for example, $U_i U_i$) is summed over all the directions of the coordinate system. Thereafter, we apply the Reynolds decomposition: $\mathbf{U} = \mathbf{u} + \mathbf{u}'$, take the inner product of the equation with the velocity $\mathbf{U} = (U_1, U_2, U_3)$ and apply the averaging rules. The resulting balance for the velocity fluctuations squared, $\mathbf{u}' \cdot \mathbf{u}' = u_i'^2$, correspond to twice the balance of the kinetic energy of the turbulent fluctuations (TKE). Under homogeneous condition

(no fluxes of TKE in space) the following four terms show up in the balance

$$\frac{1}{2}\frac{\partial\overline{(u_i')^2}}{\partial t} = -\overline{u_i'u_j'}\frac{\partial u_i}{\partial x_j} - \overline{\rho' u_3'}\frac{g}{\rho} - \nu\overline{\left(\frac{\partial u_i'}{\partial x_j} + \frac{\partial u_j'}{\partial x_i}\right)\frac{\partial u_i'}{\partial x_j}}$$

$$(I) = (II) + (III) + (IV) .$$

The interpretation of the four terms is as follows:

- (I) = rate of change of the TKE;
- (II) = rate of production (source) of TKE, $J_R = -\overline{u_i'u_j'}\frac{\partial u_i}{\partial x_j}$;
- (III) = turbulent buoyancy flux, $J_B = \frac{g}{\rho}\overline{\rho' u_3'}$;
- (IV) = turbulent kinetic energy dissipation, ε, which is always a sink of energy due to viscosity.

Under steady, homogeneous conditions and horizontal flow, the TKE reads

$$J_R = -\overline{u'w'}\frac{\partial u}{\partial z} = J_B + \varepsilon .$$

This is the most simple situation of a TKE balance. On the left, J_R, is the production term of TKE. As shown above, its source is the Reynolds stress acting on the background shear. The production J_R is equal to the so-called buoyancy flux J_B (change of potential energy in the flow field) plus dissipation ε of TKE. In the following this TKE balance equation will be applied to the surface and to the bottom boundary layer.

Using the eddy diffusivity formulation, the density flux can be rewritten as

$$\overline{\rho'w'} = -K_\rho\frac{\partial\rho}{\partial z} ,$$

with K_ρ the diapycnal diffusivity. Introducing the definition for the stability $N^2 = -(g/\rho)\frac{\partial\rho}{\partial z}$ (also known as the Brunt-Väisälä frequency), shows the relation between the change (here increase) of the potential energy J_B and the diffusivity and stability

$$J_B = \frac{g}{\rho}\overline{\rho'w'} = -K_\rho\frac{g}{\rho}\frac{\partial\rho}{\partial z} = K_\rho N^2 .$$

If the relationship between ε and J_B is known or given, e.g., $\gamma_{mix} = J_B/\varepsilon$ with γ_{mix} the mixing efficiency, the diapycnal diffusivity can be calculated from

$$K_\rho = \frac{J_B}{N^2} = \frac{\gamma_{mix}\,\varepsilon}{N^2} .$$

Therefore, measurements of ε and N^2 can yield important information about the diapycnal diffusivity. The mixing efficiency γ_{mix} is generally not constant ($\gamma_{mix} \approx$

$0.05 - 0.2$) and not a well-known function (Ivey and Imberger (1991); Ivey et al. (2008); Bouffard and Boegman (2013)).

Stratification suppresses turbulence in the vertical direction. At very small scales (<0.1 m), stratification plays a subordinate role, and viscosity (ν) and dissipation (ε) are the relevant physical quantities. Larger eddies, however, feel the stratification (N^2) and influence turbulence and the form of the spectra. For a given density stratification N^2, a vertical eddy of size L can therefore develop, if the TKE is sufficient to feed the required power to the eddy, i.e., if $L^2 N^3 < \varepsilon$. The maximum eddy size, called the Ozmidov length scale L_o, is therefore $L_o = \sqrt{\varepsilon / N^3}$. Length scales larger than L_o are influenced by stratification and turbulence at these length scales is not isotropic. The range $L \approx [L_o - 10 L_o]$ is called the buoyancy range. It is located in the spectra between the internal wave range at larger scales and the inertial and dissipation range at smaller scales.

2.3 *Vertical Structure of Wind-Induced Surface Boundary Layers*

The most crucial parameter governing the wind-driven regime is the surface shear stress τ, the force per unit area, acting on the water surface as a result of the wind. The source of this stress can be interpreted as the downward eddy-transport of horizontal momentum, $\tau = \rho_{air} \overline{U'W'}$, from the atmosphere. The concept of constant stress calls for the same Reynolds momentum flux right at the surface, $\tau = \rho \overline{u'w'}$, in the underlying water, where U, W (u, w) are the horizontal and vertical velocities of air (water), ρ_{air} (ρ) is air (water) density, and (prime) denotes fluctuations. The constant stress assumption holds for quite some height in the atmosphere and over some extent (several meters) into the SBL.

The conservation of momentum right at the interface implies that τ is equal on both sides of the interface. Owing to the presence of waves, the momentum flux into the SBL, τ_{sbl} is smaller than the applied stress τ from the air, see Fig. 2. Part of τ is consumed by the acceleration and maintenance of waves (so-called wave stress τ_{wave}), whereas the remaining momentum flux τ_{sbl} is forcing the SBL water underneath the waves. The conservation of momentum at the interface implies that the two momentum fluxes on the water-side add to the total wind stress, $\tau = \tau_{sbl} + \tau_{wave}$. This formulation indicates that waves act as a second pathway for the momentum transfer to the water. As a consequence, the wind stress, which is usually parameterized by $\tau = \rho_{air} C_{10} U_{10}^2$, using the wind drag coefficient C_{10}, depends not only on the wind speed U_{10} (measured at standard 10-meter height above the surface, but also on the presence and state of the surface waves. In fact, the wave field is crucial for the amount of momentum transferred into the water and for its vertical distribution within the SBL.

The Law-of-the-Wall A wind speed U_{10} creates a stress τ (constant stress layer), given by the Reynolds stress. Based on similarity scaling, the vertical gradient of

the horizontal velocity depends on the stress and the distance h (here h is the height above the ground or water surface; positive upward) to the surface as follows:

$$\frac{\partial U}{\partial h} = \frac{\sqrt{\tau/\rho_{air}}}{k\,h} .$$

An alternative explanation is provided by the Prandtl assumption. This equation is known as the Law-of-the-Wall and $k = 0.41$ is the von Kármán constant (experimental value). Integration leads to the well-known logarithmic wind profile

$$U(z) = U_0 + \frac{w_*}{k} \ln(\frac{h}{h_0}) .$$

For the wind-induced stress in the SBL, the above arguments can be repeated (with z now the depth, positive downward)

$$\frac{\partial u}{\partial z} = -\frac{\sqrt{\tau_{sbl}/\rho}}{k\,z} ,$$

$$u(z) = U_0 - \frac{u_*}{k} \ln(\frac{z}{z_0}) ,$$

where z_0 is the water-side roughness and u_* is the friction velocity in the SBL of the water. The rate of production of TKE, J_R, is given by the vertical divergence of the energy flux. Within the boundary layer, where the stress is constant ($\frac{\partial \tau_{sbl}}{\partial z} = 0$), this results in

$$J_R = -\overline{u'w'}\frac{\partial u}{\partial z} = -\frac{\tau_{sbl}}{\rho}\frac{\partial u}{\partial z} .$$

After inserting the definition of u_*, the production of TKE in the logarithmic boundary layer is given by

$$J_R = u_*^2 \frac{\sqrt{\tau_{sbl}/\rho}}{k\,z} = \frac{u_*^3}{kz} .$$

According to Ficks second law, the rate of change of TKE is given by the vertical divergence of the energy flux (J_R, source term), minus dissipation (ε, sink term), minus buoyancy flux (J_B, sink term). For isotropic and steady-state turbulence, the production J_R of TKE must be in equilibrium with the dissipation ε and the buoyancy flux J_B, i.e. $J_R = \varepsilon + J_B$. If the boundary layer is not density-stratified (i.e. the boundary layer is homogeneous and therefore $J_B = K_z N^2 = 0$), the following equation results for the energy dissipation ε:

$$\varepsilon = J_R = \frac{u_*^3}{k\,z} .$$

If the wave-induced stress, τ_{wave}, is small, then $\tau \approx \tau_{sbl}$ and the dissipation can be expressed in terms of the wind forcing: $\tau_{sbl} = \rho u_*^2 = \rho_{air} C_{10} U_{10}^2$, with U_{10} the wind speed measured at 10 m above the water surface,

$$\varepsilon = \left(\frac{\rho_{air}\ C_{10}}{\rho}\right)^{3/2} \frac{U_{10}^3}{kz} .$$

The level of wind-induced turbulence as a function of depth z can be estimated based only on the wind speed U_{10}. The most detailed turbulence measurements in the ocean, performed with the dissipation method, are consistent with $\varepsilon \propto U_{10}^3$ and follow the empirical relation

$$\varepsilon \simeq 1.8 \left(\frac{\rho_{air}\ C_{10}}{\rho}\right)^{3/2} \frac{U_{10}^3}{kz} .$$

The factor 1.8 includes much uncertainty, as C_{10} is not well defined. Despite this uncertainty, the level of turbulent dissipation in a wind-induced surface boundary layer is therefore quite well defined.

Viscous boundary layer Due to wave breaking, the very top layer as well as the very last millimeters of the transition from water-to-air is not well defined. One can think of a well-defined boundary layer with molecular/laminar interfaces interrupted regularly by breaking waves, where the contact between water and air is torn in pieces and bubbles enhance the contact surface between air and water by orders of magnitudes. During those short moments, the contact between water and air is much intensified. After a few seconds the boundary layer is again established and the contact between water and air is back to normal (weak, molecular bottleneck). The thickness δ_ν, where the turbulent eddy viscosity K_{turb} falls below the kinematic viscosity ν, defines the viscous boundary layer (VBL). Within this sublayer, the viscous forces dominate the resistance to momentum transfer. Subsequently in the viscous sublayer the greatest changes in velocity occur and the horizontal flow becomes laminar. The shear stress τ is still equal to the (constant) stress above, but the momentum flux becomes now only a function of the (molecular) viscosity. Therefore, with $\tau_{sbl} = \rho\nu \frac{\partial u}{\partial z}$ we obtain

$$\frac{\partial u}{\partial z} = \frac{u_*^2}{\nu} ,$$

and the shear gradient depends only on the (friction) velocity and the viscosity. The distance from the bottom—where the flow is laminar—is given by $\delta_\nu \approx 10\nu/u_*$. The same arguments apply for the air-side and one can define a VBL on the atmospheric side.

Diffusive boundary layer and gas exchange velocity Following the same argumentation as above for the specific case of the turbulent eddy viscosity K_{turb}, the turbulent diffusivity is decreasing as the air-water interface is approached and at some small distance from the interface the turbulent diffusivity would fall below the

molecular diffusivity D_c. As diffusivity can never drop below the molecular diffusivity, we define the layer of only molecular flux through the interface (Ficks first law)

$$J_C \;=\; -D_C \frac{\partial C}{\partial z} \;\approx\; \frac{D_C}{\delta_{dbl}} \Delta C \;=\; V_{tot}\; \Delta C \;,$$

as the diffusive boundary layer (DBL) with thickness δ_{dbl}. The DBL thickness is slightly solute-specific because δ_{dbl} depends on D_c which is substance (C) and temperature dependent. The gas exchange is often characterized by the piston velocity $V_{tot} = D_c/\delta_{dbl}$, which in the literature is called gas exchange velocity or mass transfer velocity/coefficient. As indicated by the previous equation, $V_{tot} = D_c/\delta_{dbl}$ includes two influences: (i) the molecular properties of the substance C and (ii) the effect of the wind forcing expressed by δ_{dbl}. Therefore, V_{tot} depends on the substance, the temperature and the wind.

Wave dependency of wind-induced stress The total surface stress is usually parameterized by the drag coefficient C_{10}, which quantifies the total vertical momentum flux τ well above the wave-affected boundary (at standard 10 m height). The experimental data show a large scatter, but nevertheless, there is a relatively clear conceptual picture. The drag coefficient depends to large extent only on wind speed and the wave development state.

From these two factors, we consider first the situation of developed waves at different wind speeds. There are basically two ranges to be considered: wind larger than 5 ms^{-1} and wind below 5 ms^{-1}. For strong winds (>5 ms^{-1}) the surface roughness is determined by the height of the gravity waves, and subsequently, friction is dominated by those waves. The wind speed depends on the measurement height z as

$$U(z) \approx w_* \left(k^{-1} \ln \left(\frac{gz}{w_*^2} \right) + K \right)$$

for different wind velocities ($k = 0.41$ is the Von Kármán constant). The denominator w_*^2/g is the so-called waveheight scale, which represents a measure of the roughness of the surface waves. The constant K is relatively universal and has been determined to be $K \approx 11.3$. Introducing this function of $U(z)$ into the definition of C_{10} allows determining C_{10} by

$$C_{10} \approx \left(k^{-1} \ln \left(\frac{10g}{C_{10} U_{10}^2} \right) + K \right)^{-2} .$$

This equation is an implicit relation in C_{10}, converging quickly after about four iterations. The typical values of C_{10}, see Fig. 3, range from 0.0011 (at $U_{10} = 5\,\mathrm{ms}^{-1}$) to 0.0021 (at $U_{10} = 25\,ms^{-1}$).

For weak winds (<5 ms^{-1}) the influence of gravity waves on surface stress eases, and surface tension or small-scale capillary waves, generating virtual roughness, become increasingly important. At low wind, one could expect the smooth law

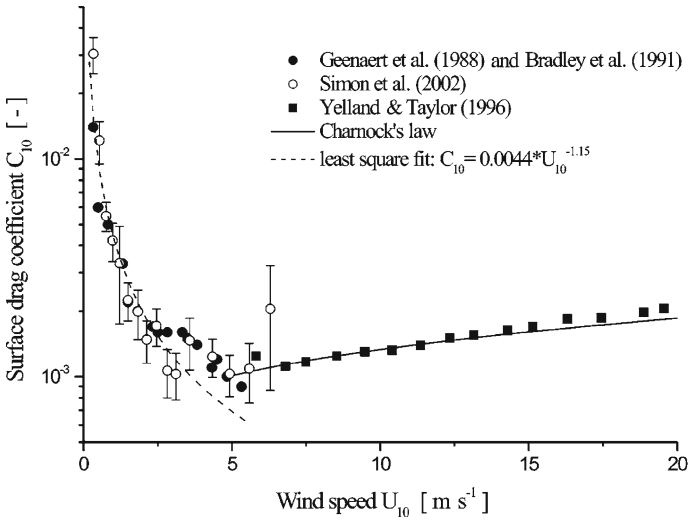

Fig. 3 Wind-drag coefficients C10 for developed waves as a function of wind speed U10 at standard (10 m) height above water. Courtesy of Wüest and Lorke (2003)

$U(z) = w_*(k^{-1}\ln(w_* z \nu_{air}^{-1}) + 5.7)$ to apply (where ν_{air} is the kinematic viscosity of air). Indeed, for wind velocities of 3 to 5 ms^{-1}, see Fig. 3, experimental evidence confirms the smooth-law value for $C_{10} \sim 0.001$. However, at even lower wind ($<3\,ms^{-1}$), the experimental values of C_{10} consistently increase much faster (Fig. 3) with decreasing wind compared to the smooth-law prediction. According to the data shown in Fig. 3, the empirical parameterization $C_{10} \approx 0.0044 U_{10}^{-1.15(\pm 0.09)}$ (with U_{10} in ms^{-1}) for wind speeds less than $3\,\mathrm{ms}^{-1}$ can be used. Astonishingly enough, such weak winds have drag coefficients larger than those for $25\,\mathrm{ms}^{-1}$ winds. In lakes, the light-wind C_{10} value is of great relevance because most inland waters (especially small-to-medium-sized lakes) are exposed for most of the time to light winds only.

The above C_{10} approximations represent lower bounds because they are based on developed wave fields. For young, accelerating, and breaking waves, the friction, and thereby also C_{10}, will be larger than in Fig. 3.

Langmuir circulation In addition to wind-induced small-scale turbulence, an organized vertical motion of the scale of the epilimnion depth also evolves under the action of surface wind-stress. The hydrodynamics of these vortices, termed Langmuir cells, is not simple. We refer to Leibovich (1983) for an overview of the relevant theories and more detailed description.

When the wind speed exceeds a certain threshold speed of $\sim 3\ \mathrm{ms}^{-1}$, within a few minutes, streaks, aligned approximately parallel to the wind direction and composed of floating objects such as bubbles and leaves can develop on the lake surface. As Langmuir (1938) showed, these streaks result from the convergence of two counter-rotating vortices at the top of the epilimnion with axes nearly parallel to the wind. Hence, surface water is transported downward at the streaks and upwelling

occurs in between. This circulation pattern establishes itself independently of surface heating or cooling. A destabilizing surface heat flux may lower the threshold for the onset of these convective rolls.

The form of the rolls is asymmetric, but the lateral width (approximately half of the streak spacing L; see Fig. 2) and the vertical penetration depth of the rolls are observed to be approximately equal. Generally, the spacing L of the streaks increases with wind speed U_{10} and can be approximated according to Leibovich (1983) by: $L \sim (2 - 5\mathrm{s}) \times U_{10}$.

However, the vertical scale of the circulation is limited by the base of the mixed layer, where strong density gradients suppress vertical motion. Thus, the above equation can only hold as long as $L/2$ is smaller than the epilimnion depth. Hence, the wind threshold and the epilimnion depth put lower and upper limits on the size of the Langmuir vortices. In fact, the size of the cells in lakes is mostly on the order of 10 m.

Downwelling at the convergence streaks can attain maximum vertical velocities of ~1% of the wind speed. The structure of the rolls is asymmetrical, with downwelling currents being of higher velocity than the upwelling currents. In general, downwelling velocities increase with wind speed and are comparable to the wind-induced surface drift. The downwelling velocities suggest that Langmuir circulation may cause epilimnion mixing. While observations led Langmuir (1938) to believe that the vortices are responsible for the formation and maintenance of the mixed layer, at present it is not certain whether Langmuir circulation is responsible for a significant part of the stirring. Nevertheless, Langmuir cells are important for the ecology of surface waters, since the environment to which an algal cell is exposed—especially light intensity—depend critically on whether or not it is undergoing vertical transport by such vortices.

2.4 Vertical Structure of the Bottom Boundary Layer

The bottom boundary layer (BBL) follows the same concept as the SBL with more simple boundary conditions. The transition from the background flow, far away from the sediment, to the flow at the sediment/water interface is less complex than in the SBL because of the absence of waves, the lower variability of the forcing, and the rigid boundary (zero velocity). The temporal structure of the BBL is also steadier than the SBL, owing to the different nature of the forcing. Whereas the SBL is exposed to fluctuating wind stress, the BBL is defined by friction, which damps unsteady currents and removes fluctuations. Nevertheless, there are many similarities between the BBL and SBL. The BBL of lakes is usually actively turbulent, with the exceptions of small and wind-protected lakes, where strong stratification can reach all the way to the sediment.

The BBL can be split up into three different layers, see Fig. 5: the logarithmic layer, where the flow is turbulent and the Law-of-the-Wall is mostly applicable, the

viscous boundary layer (VBL), where the flow becomes laminar due to viscosity, and the diffusive boundary layer (DBL), where fluxes are limited by molecular diffusion.

The bottom stress τ_{bbl}—here assumed again to be constant through the BBL—defines the friction velocity $u_* = \sqrt{\tau_{bbl}/\rho}$, the characteristic velocity scale within the BBL (imagine as the velocity of the turbulent eddies in the BBL). In the turbulent logarithmic layer, the TKE balance is given by production = dissipation (assuming negligible BBL stratification, $N^2 = 0$); i.e.,

$$J_R = -\overline{u'w'}\frac{\partial u}{\partial z} = \frac{\tau_{bbl}}{\rho}\frac{\partial u}{\partial z} = \varepsilon \, .$$

We assume again (as in the SBL), that the eddy viscosity satisfies Prandtl's mixing length hypothesis where the eddy sizes and diffusivity increase with distance h to the wall. This leads also here to the Law-of-the-Wall with $\frac{\partial u}{\partial z} = u_*/kh$ and $\varepsilon = u_*^3/kh$. Current measurements in lakes indeed match these relations with stunning agreement. In the example presented in Fig. 5, 8.5 min averages of the currents follow the logarithmic profile over several meters within the BBL.

In the BBL the energy dissipation (kinetic energy loss) is due to bottom friction. The dissipation—in steady state—is equal to the total energy flux into the BBL. The dissipation within the layer from the sediment to 1 m above the sediment is given by

$$P_{diss,1m} = \tau_{bbl}U_{1m} = \rho C_{1m}U_{1m}^3 = \frac{\rho}{C_{1m}^{1/2}}u_*^3 \, .$$

In weakly forced water bodies the low turbulence level may not be able to keep the BBL well mixed. The continuous release of dissolved solids from the sediment (by mineralization and other sediment processes) can stabilize the BBL ($N^2 > 0$) and suppress mixing. In this case, the Osborn model for the eddy viscosity can be used, $K_\nu = \gamma_{mix}\varepsilon N^{-2}$ which is a function of the distance from the sediment. In contrast to the well-mixed case, K_ν is increasing toward the sediment until the distance $h \approx \sqrt{\gamma_{mix}}u/(kN)$ is reached. Below this critical height, the diffusivity is decreasing again according to Law-of-the-Wall and even faster close to the sediment.

The diffusivity K_ν is the sum of the molecular diffusivity and turbulent eddy diffusivity, K_{turb}. Compiling the many parameterizations for K_{turb} reveals that it decreases steeply as h^3 to h^4 when approaching the sediment. Subsequently, there are two heights where K_{turb} becomes smaller than the molecular viscosity and the molecular diffusivity, see Fig. 4, respectively. The height δ_ν, where K_{turb} falls below the kinematic viscosity, defines the top of the viscous boundary layer (VBL). Within this sublayer, the viscous forces dominate the resistance to momentum transfer. Subsequently in the viscous sublayer the greatest changes in velocity occur and the horizontal flow becomes laminar. The boundary-layer thickness δ_{bbl} is still equal to the constant value above, but the momentum flux is only a function of the (molecular) viscosity. Therefore,

$$\frac{\partial u}{\partial z} = \frac{\tau_{bbl}}{\rho\nu} = \frac{u_*^2}{\nu}$$

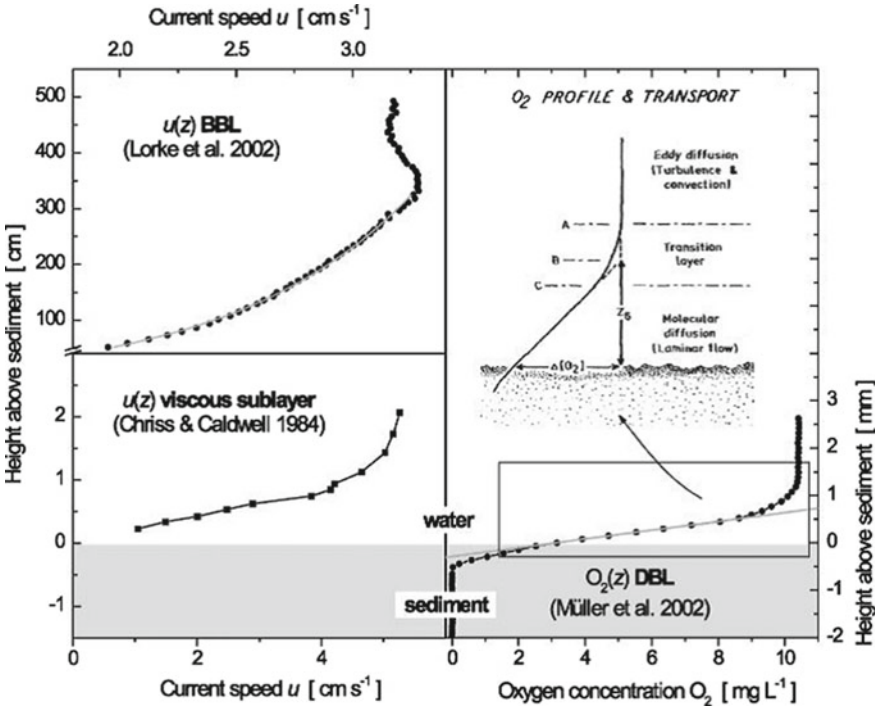

Fig. 4 Measured seiching currents (*upper left*), showing a perfect BBL logarithmic layer in a lake, from Lorke et al. (2002), and deep ocean currents (*lower left*), exemplifying the linear profile in the viscous sublayer, from Caldwell and Chriss (1979). The oxygen profile is on a sub-mm scale and shows the 0.7 mm thick diffusive boundary layer in a lake, from Mueller et al. (2012) *lower right*). The schematic, adapted from Jorgensen and Des Marais (1990), defines the outer limit (*A*), the true (*C*), and the effective (*B*) diffusive boundary layer (typically 1 mm thick; *upper right*). The transition layer (broken line) is also perfectly identifiable in the oxygen micro-gradient (*lower right*). Courtesy of Wüest and Lorke (2003)

and the gradient depends only on the friction velocity and the viscosity. The distance from the bottom—where the flow becomes laminar—is given by $\delta_\nu \approx 10\nu/u_*$, typically millimeters to centimeters, see Fig. 4. Within the viscous sublayer, turbulent eddies are virtually absent. The Reynolds number $Re = u\delta_\nu/\nu$ is only of order 100 or smaller and therefore indicates no turbulence. The flow in the viscous sublayer is practically laminar. In the viscous boundary layer, turbulent kinetic energy dissipation is at its maximum, even though the flow is laminar. The TKE balance, leads to

$$\varepsilon_\nu = \frac{\tau_{bbl}}{\rho}\frac{\partial u}{\partial z} = \frac{u_*^4}{\nu}\,.$$

The dissipation in the VBL increases with the power 4 with the friction velocity—as to be confirmed easily by dimensional analysis. Hence the total dissipation in the viscous sublayer is given by

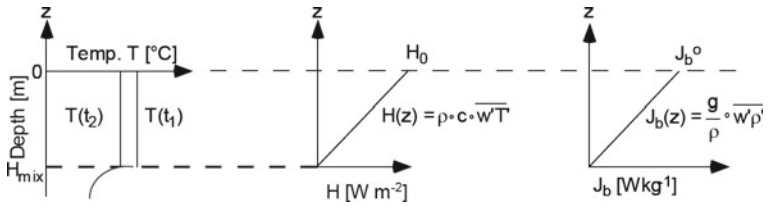

Fig. 5 Schematics of the heat flux (*middle*) and the buoyancy flux (*right*) as an effect of homogeneous cooling of a mixed SBL (*left*)

$$P_{diss}^{\nu} = \rho\varepsilon_{\nu}\delta_{\nu} = \frac{\rho}{\nu}u_*^4\delta_{\nu} \approx 10\rho u_*^3 \,.$$

Comparing the total VBL dissipation with the total BBL dissipation, provides a ratio of $P_{diss}^{\nu}/P_{diss} = 10C_{1m}^{0.5} \approx 0.4$. Thus, about 40% of the total energy entering the BBL is dissipated within the VBL (laminar), the remainder being dissipated within the logarithmic layer (turbulent). The practical implication is, that about 40% of the energy dissipation in the BBL is laminar (causing no mixing), whereas about 60% is turbulent (causing mixing).

Analogously, $K_{turb} \sim D_c$ defines the top of the diffusive boundary layer (DBL) (Fig. 4), which extends, according to the z-dependence of K_{turb} to $\delta_D \approx \delta_{\nu}(D_C/\nu)^a$ (a is between 1/4 and 1/3). Since molecular diffusivity is about three orders of magnitude lower than viscosity, the thickness δ_D is about 10 times smaller than δ_{ν}. Within the DBL, transport by eddies becomes insignificant compared to molecular diffusion.

The diffusive bottom boundary layer As evidenced from the first Fick law, $D_C\partial C/\partial z \approx (D_C/\delta_{dbl})\Delta C$, the key parameter for the sediment/water flux of a solute C is the gradient within the DBL. Those gradients depend on the thickness δ_{dbl} and the rate of consumption (or production) of solute C in the sediment, the latter affecting the concentration driving force ΔC across the interface. The DBL thickness is solute-specific because δ_{dbl} depends on D_C (varying by a factor of ~2 among the different solutes) and is slightly temperature-dependent, as ν and D_C are both functions of temperature.

The DBL thickness is not well defined for several reasons. Most obviously the top end of the DBL (in fact also the top of the VBL) is not sharp, because the turbulence cut-off at the Kolmogorov scale $\eta = (\nu^3/\varepsilon)^{1/4}$ is a gradual roll-off following the turbulence spectrum ~ (eddy size)$^{-b}$ with $b = 3 - 4$. Therefore, a transition zone exists between the pure molecular and fully turbulent zones above, where K_{turb} and D_C are approximately equal. To remove this ambiguity, the effective DBL is defined by extrapolating the linear concentration gradient right above the sediment to the bulk water concentration, see Fig. 4. This theoretical DBL thickness provides a practical procedure to calculate the true flux through the interface based on ΔC, the concentration difference between the sediment surface and the bulk water above.

The relevance of the deep currents for the sediment/water transfer of solutes becomes more obvious by expressing the molecular flux by the mass transfer coefficient (D_C/δ_{dbl}). Because the mass transfer coefficient is $\frac{D_C}{\delta_{dbl}} = \nu/\delta_\nu \sim u_*$, the interfacial flux becomes proportional to the flow acting on the BBL. As a practical consequence, wind-exposed aquatic systems will show higher rates of degradation and turnover of organic matter than weakly forced ones. As a global consequence, old lacustrine sediments contain more organic carbon and nutrients than relic marine sediments. Besides the molecular DBL fluxes, there are additional pathways between the sediment and water. In Lake Erie, for instance, zebra mussels have created densely populated reefs (with several thousand mussels per m^2), which have been identified for their enormous venting capacity. As another example, in shallow waters, heating of the sediments by short-wave radiation causes buoyant porewater to convect through the interface. Such nonlocal processes are often more effective than molecular diffusion. In eutrophic waters, advective transport through the sediment-water interface occurs mainly by methane and carbon dioxide bubbles formed in the anoxic sediment. Whereas in oligotrophic lakes, where the sediment surfaces remain oxic, worms or other macrofauna (such as insect larva) act as conveyor belts through the interface and produce ventilation dips and mounds. The biotic invasion has a positive feedback effect: Enhanced activities of macro- and meiofauna, which move sediment around and pump oxygen-rich water into their burrows, improve the oxic conditions in the sediment and thereby improve the living conditions for more bottom biota. Bioturbation by benthic organisms, therefore, is of general importance for the distribution and flux of soluble and colloidal material in lacustrine sediments. Besides the direct effect on the flux of matter between sediments and water, biota has an indirect effect on the ex-change by influencing the BBL roughness. Faecal pellets, tracks, trails, tubes, pits, and mounds enhance the structuring and spatial heterogeneity and increase the bottom roughness, leading to an increase in the mass and momentum transfer.

2.5 Convectively-Induced Turbulence and Mixing in the Boundary Layers

Convectively-driven turbulence occurs in natural waters under several circumstances:

1. Cooling-induced turbulence in the surface boundary layer (SBL)
2. Warming-induced turbulence in the bottom boundary layer (BBL)
3. Convective turbulence caused by thermobaric-instabilities
4. Local instabilities caused by double diffusion
5. Shear-induced convective instabilities in the bottom boundary layer (BBL).

These occasions are the classical examples, however, there are more possibilities. In general, convective turbulence occurs when some density-modifying processes manoeuvre or produce heavier water on top of lighter water. Further examples are: (i) evaporation in salty waters causing higher salinity/higher density at the very top

of the water body; (ii) the release of bubbles at the sediment—reducing density at the bottom of the water column.

Surface boundary layer convective turbulence In the boundary layer near the surface (SBL) convection occurs, when higher density is produced at the very top (right at the surface) of the water column. Higher density is produced by cooling when $T > T_{MD}$ (temperature for maximum density) or by salinity-production via evaporation. As a result, the surface water column becomes unstable and convective turbulence sets in (Rayleigh instability). The net density (mass) flux $\overline{w'\rho'} = F_\rho$ is directed downwards (heavier parcels moving down and lighter ones moving up, see Fig. 6) and causes a contribution in the buoyancy flux term. In the TKE budget, the term $J_B = (g/\rho)\overline{w'\rho'}$ makes a positive contribution (= production of turbulence; here J_b is a source of turbulence).

The most common way to generate heavier water parcels at the top is by cooling the SBL (loss of heat to the atmosphere). The effect of cooling is the formation of small parcels right at the top of the surface which are slightly cooler than the parcel below. If $T > T_{MD}$ then the slightly cooler parcels are also slightly heavier by $\Delta\rho$ and subsequently sink. Relative to the base of a mixed layer (of thickness h_{mix}), these

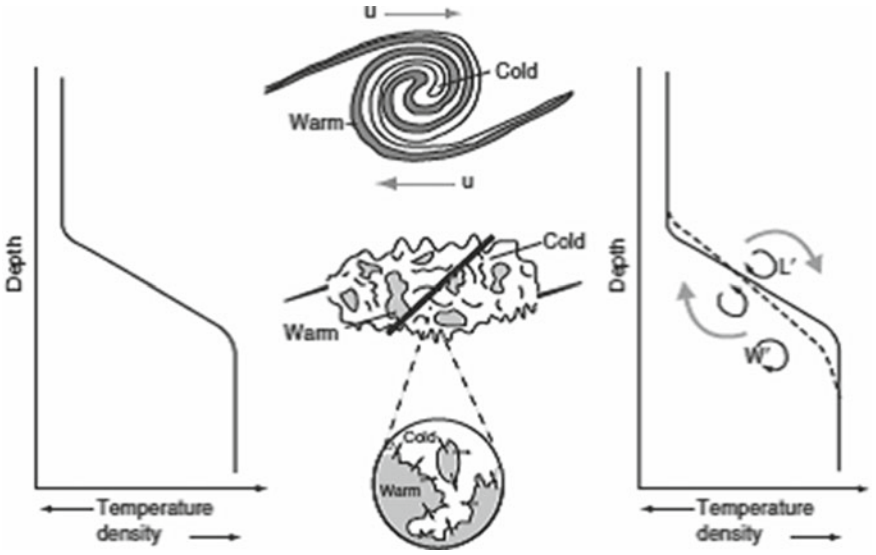

Fig. 6 The effect of turbulent mixing in a stable stratification: if the vertical gradient of horizontal currents (current shear) is stronger than the stability of the water column, Kelvin-Helmholtz instabilities can develop (*top* of *middle* panel) bringing warmer (lighter) and cooler (heavier) water in close proximity (*bottom* of *middle* panel). Finally, heat (or any other water constituent) is mixed by molecular diffusion across the manifold small-scale interfaces, which are generated by turbulence (see inset). The turbulent exchange of small water parcels leads to a fluctuating vertical heat flux which averages to a net downward heat flux. As a result, the original temperature profile (*left*) is modified (*right*): the vertical gradient is weakened and expanded vertically with heat transported from *top* to *bottom* across the interface. Courtesy of Wüest and Lorke (2009)

parcels have a potential energy (per kg of parcel mass) given by $(gh_{mix}/\rho)\Delta\rho$, where $\Delta\rho$ is the density difference of the water parcel relative to the background density. We assume that the "density producing process" lasts for some time. Then we can express the potential energy production per time interval Δt (rate of potential energy production) as $(gh_{mix}/\rho)\frac{\Delta\rho}{\Delta t}$. Because the density and potential energy production occurs right at the very top, we call this production term in the following as (index o for surface and b for buoyancy), the surface buoyancy flux,

$$J_B^o = \frac{gh_{mix}}{\rho}\frac{d\rho}{dt} .$$

This equation can intuitively be interpreted. Assume that the sinking parcels have a higher density by $\Delta\rho$. They replace lighter water parcels below (ρ) until the entire mixed layer has a density of $\rho + \Delta\rho$. We assume that the time interval Δ_t is needed to replace all the parcels of the mixed-layer with water of density $\rho + \Delta\rho$. One can think of a front of higher density water moving downwards with a velocity of $w = -h_{mix}/\Delta t$ with an associated density flux $F_\rho = w\Delta\rho$. For a mixed layer of thickness h_{mix} and a rate of density increase of $d\rho/dt$, the change of potential energy per area of the entire mixed layer is given by

$$F_{pot} = \frac{gh_{mix}^2}{2}\frac{d\rho}{dt} ,$$

where the factor 1/2 is due to the vertical integration of hdh over the entire mixed layer h_{mix}. Using the definition of J_B^o (above) leads to the following relation between F_{pot} and J_b^o:

$$F_{pot} = \frac{h_{mix}\rho}{2}J_b^o .$$

Cooling-induced convective turbulence The TKE balance in the non-stratified and non-sheared SBL (i.e. no other turbulence sources than convection; no large-scale shear) has a simple form, $\varepsilon = J_B = (g/\rho)\overline{w'\rho'}$.

In Fig. 5, the buoyancy flux is schematically shown for a mixed layer loosing heat while cooling from temperature $T(t_1)$ to $T(t_2)$. For a homogeneous rate of cooling $\frac{\partial T}{\partial t} = \frac{T(t_2)-T(t_1)}{\Delta t}$ within the mixed-layer of thickness h_{mix} the vertical heat flux as a function of depth is given by

$$H(z) = c_p\rho\overline{w'T'}(z) = c_p\rho\frac{\partial T}{\partial t}(-h_{mix} - z) .$$

Temperature T and density ρ are connected via the expansion coefficient α via $\frac{\partial\rho}{\partial T} = -\rho\alpha$. The same holds for the fluctuations, $\rho' = -\rho\alpha T'$. Therefore, the heat flux $H(z)$ and the buoyancy flux $J_B(z)$ are directly related by

$$J_B = \frac{g}{\rho}\overline{w'\rho'} = -\frac{g}{\rho}\alpha\rho\overline{w'T'} = -\frac{\alpha g}{c_p\rho}H(z) .$$

The heat flux $H(z)$ is positive upwards and ρc_p is the heat capacity. For the example in Fig. 6, where $H(z)$ is linear in z and also $J_b(z)$ is therefore a linear function with depth,

$$J_B(z) = \alpha g \frac{\partial T}{\partial t}(-h_{mix} - z) \; .$$

The average dissipation ε within the mixed layer h_{mix} is therefore $0.5 J_B^o$, as follows directly from inserting the above relations into the definition of the average,

$$\overline{\varepsilon} = \frac{1}{h_{mix}} \int_{h_{mix}}^{\varepsilon} (z) dz = \frac{1}{h_{mix}} \int_{h_{mix}}^{J_b} (z) dz = \frac{1}{h_{mix}} \frac{g\, h_{mix}^2}{2\rho} \frac{d\rho}{dt} = \frac{1}{2} J_B^0 \; .$$

It implies that the average dissipation is a function of the surface buoyancy flux alone. As a consequence, there are only two relevant physical parameters defining the similarity scaling for convective turbulence: thickness h_{mix} and surface buoyancy flux J_B^o.

Sources of buoyancy flux The buoyancy flux is a source or sink term in the turbulent kinetic energy (TKE) balance. The sign of the buoyancy flux has the following meaning for the TKE balance:

- $J_B^o > 0$: Production of TKE (i.e., sinking heavier water parcels or rising lighter water parcels), $J_B(z) > 0$ in the entire SBL.
- $J_B^o < 0$: Strengthening of stratification; no turbulence is produced, therefore $J_B(z) = 0$ in the interior.

The following processes can lead to a positive buoyancy flux and therefore to convective mixing, both at the water surface or within the water column:

1. Heat flux at the water surface (H_{net} = heat flux from the water surface to the atmosphere):

$$J_B^o = \frac{g h_{mix}}{\rho} \frac{d\rho_o}{dt} = -g h_{mix} \alpha \frac{dT_o}{dt} = \frac{\alpha g}{\rho c_p} H_{net,o} \; .$$

2. Change in salinity:

$$J_B^o = g h_{mix} \beta \frac{dS}{dt} = \frac{g\beta s}{\rho} m_E = g\beta S E = \frac{g\beta s}{\rho \lambda e} H_E \; .$$

Here, $\beta \sim 0.8 \times 10^{-3} ‰^{-1}$: coefficient of haline contraction, S = salinity, λ_e = specific latent heat; H_E = latent heat flux, m_E = evaporation rate, E = evaporation. Increasing salinity at the surface increases density and generates turbulence ($J_b^o > 0$). Decreasing surface salinity leads to a negative buoyancy flux. E must then be replaced by precipitation, ice melting, or freshwater addition (inflow).

3. Heat fluxes through the water-sediment boundary ($H_{net,B} > 0$ means heat flux into the water, index b for bottom):

$$J_B^b = -\frac{gh_{mix}}{\rho}\frac{d\rho_b}{dt} = gh_{mix}\alpha\frac{dT_b}{dt} = -\frac{\alpha g}{\rho c_p}H_{net,b} \ .$$

4. Remineralisation of salts: negative buoyancy flux, leads to stabilization.
5. Double diffusion: production of TKE by sinking salt fingers (finger regime) or rising thermals (diffusive regime).
6. Particles settling from density currents.

3 Stratified Turbulence in Lakes Interior

Below the surface boundary layer (SBL), almost all natural waters (lakes, reservoirs, estuaries, oceans) are density-stratified to some extent. The turbulence in this stratified part of the water body (stratified deep ocean; stratified hypolimnia of lakes, etc.) is strongly reduced and vertical exchange occurs over relatively short vertical scales. Large vertical eddies have not enough energy to be maintained and do not exist. Due to these short exchange lengths the vertical fluxes are more of "diffusion-type" and therefore it is adequate to quantify the fluxes by turbulent diffusivities. However, the prominent feature of the thermocline is not turbulence but the persistent existence of internal waves (which may cause turbulence, if intense enough).

Kelvin-Helmholtz instability and Richardson number The shear flow in a stratified fluid is characterized by two relevant physical quantities, shear and stability. Similar to the Reynolds number and the Rayleigh number, here again a dimensionless number is formed to characterize the phenomenon. The Richardson number is defined as the ratio of the stabilizing to the destabilizing force

$$\frac{\text{buoyancy}}{\text{inertia}} = \frac{N^2}{\Delta u^2/L^2} = Ri \ ,$$

or

$$Ri = \frac{N^2}{(\partial u/\partial z)^2} \ .$$

Two cases can be distinguished separated by the critical Richardson number $Ri_c \sim 0.25$. This critical value can be determined experimentally, as indicating the transition from stable (laminar) to turbulent flow. In the case that $Ri < Ri_c$: Kelvin-Helmholtz instability, the flow field is dominated by overturns, and the fluid flow is turbulent with enhanced vertical transport, see Fig. 6. For $Ri \gg Ri_c$: the density stratification is dominant, stability is stronger than shear, i.e., small perturbations are damped by stability and do not grow to turbulence. The energy contained in the perturbations is radiated (distributed) by internal waves.

Turbulence measurements in natural waters In the following sections, some techniques that are used to determine energy dissipation rates in natural stratified waters are briefly described. They all have in common that they rely on instruments that allow measuring either velocity fluctuations or temperature fluctuations (salinity fluctuations: today technically not yet possible) with a very high spatial and temporal resolution. The need to resolve the smallest scales that still contribute significantly to the total variance of velocity or temperature (or salt) is the major challenge. The drop-off of the spectra at high wave numbers is determined by the level of energy dissipation ε, since both the Kolmogorov k_K and the Batchelor k_B wave numbers depend on ε:

$$k_K = \left(\frac{\varepsilon}{\nu^3}\right)^{1/4},$$

$$k_B = \left(\frac{\varepsilon}{\nu D^2}\right)^{1/4}.$$

Therefore, ε determines the required spatial resolution of the measurements, see also Fig. 7. Since the maxima of the spectra are in the range of millimeters or centimeters, measurements need to be performed with such a high resolution. Consequently, the experiments are laborious and include the processing of large amounts of data. Fluctuations of temperature and velocity are sampled as time series. The wave number k is calculated from the frequency f and the sinking velocity W of the sensor (typically 0.1–1 ms^{-1}) by $k = f/W$.

Turbulence techniques—inertial dissipation method According to the discussion above, the equilibrium range consists of the inertial subrange (*left* side of the spectrum; larger scales) and the dissipation subrange (*right* side of the spectrum; smaller scales and viscous cut-off). In the inertial subrange the energy spectrum follows $\Phi(k) = a\varepsilon^{2/3}k^{-5/3}$.

The dissipation level can be determined, if the energy of the power spectrum $\Phi(k)$ can be measured in the inertial subrange. Ideally, the instrument is able to resolve the turbulence *down* to the Kolmogorov length scale. An example of a measured energy spectrum in the ocean is given in Fig. 8.

Turbulence techniques—dissipation method and shear probes Vertical profiles of horizontal velocity fluctuations u are measured using a microstructure shear probe, which can sample vertical gradients of horizontal velocity $\partial u'/\partial z$ with an accuracy of about 10^{-4} s^{-1} and a resolution on the millimeter scale. The probe is mounted at the front of a free-falling device which descends at a speed of typically 0.5–1 ms^{-1}. The dissipation rate is then directly calculated from the spectrum of the shear

$$\varepsilon = 7.5\nu\overline{\left(\frac{\partial u'}{\partial z}\right)^2} = 15\nu\int_0^\infty \Phi_S dk\ .$$

The factor 7.5 is due to the fact that only one component of the shear is actually measured.

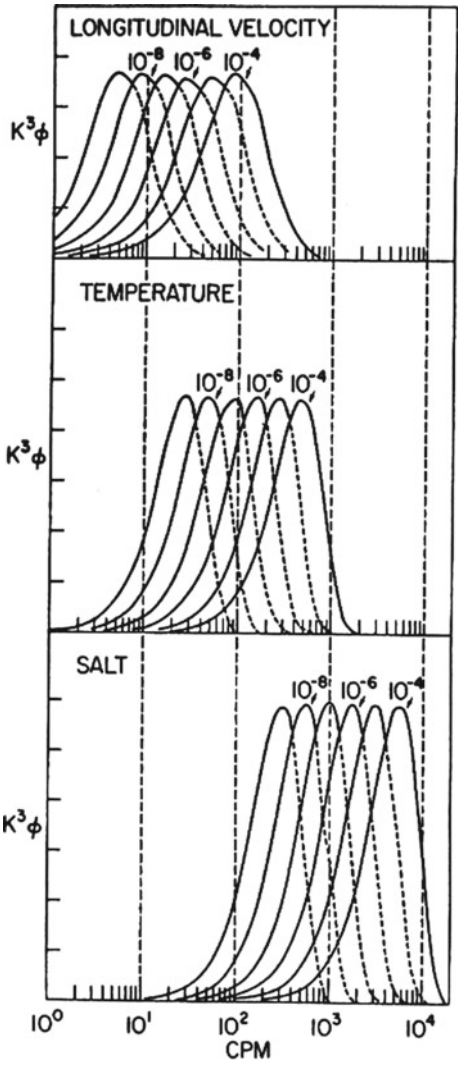

Fig. 7 Energy-preserving plot of the spectra of shear (*upper* panel) temperature gradients (*middle* panel) and salt gradients (*lower* panel). The area beneath the curves is equal to ε (shear) and χ_T (temperature) and χ_S (salt), respectively. To get accurate results, measurements need to resolve the fluctuations at least down to the scales where the maxima of the curves are located. This is in the cm or mm range for most practical applications. A device that is able to sufficiently resolve the salt gradients still needs to be developed. (CPM = cycles per meter)

Turbulence techniques—Batchelor method The Batchelor method for measuring turbulence is based on the scalar spectrum for temperature between the Kolmogorov (η) and the Batchelor (η_B) length scales. In lakes or oceans, vertical temperatures are profiled with a sufficiently high resolution to measure the smallest vertical scales of turbulence. This is performed using a free-falling microstructure probe which samples temperature at a fast rate and with a high resolution. For example, the spectrum shown in Fig. 9 was derived from data measured with a probe moving at a speed of about 0.1 ms^{-1} and sampling temperature with a frequency of 96 Hz and a resolution of 5×10^{-4} C (0.5 mK). Sections of the temperature profile are

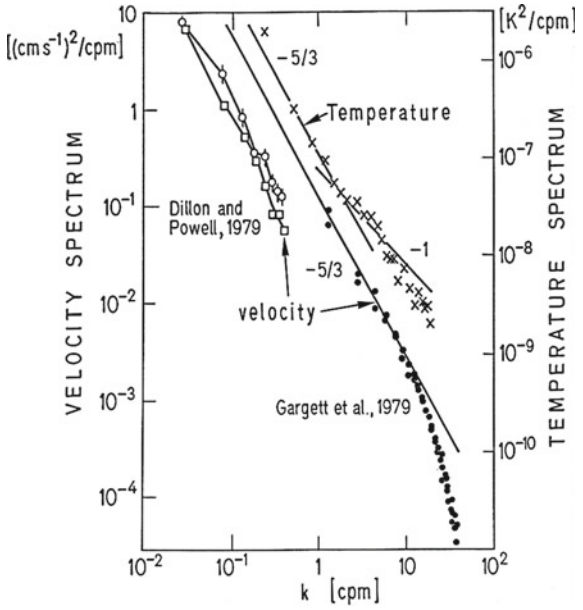

Fig. 8 Two curves on the *left* refer to energy spectra (scale on the *left* axis). Dillon and Powell (1979) refers to lake surface waters. Gargett et al. (1979) represents data from the ocean interior. In both cases, the $-5/3$ slope indicates the inertial subrange. The temperature spectrum shows the $-5/3$ and the -1 (Batchelor spectrum). Courtesy of Imboden and Wüest (1995)

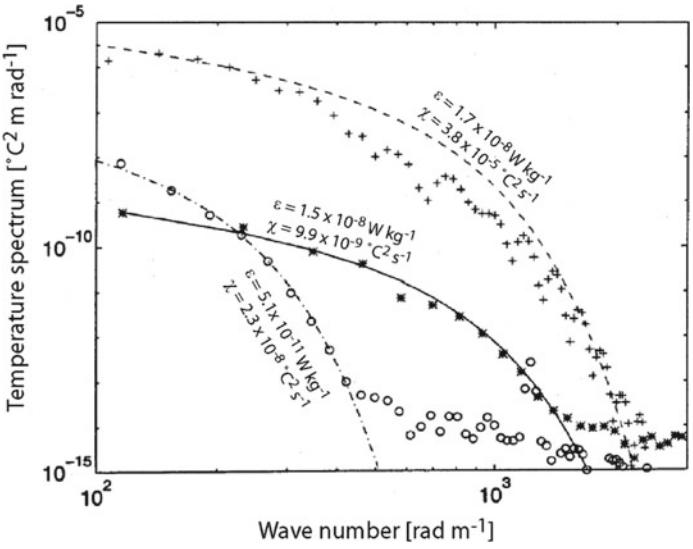

Fig. 9 Temperature spectra calculated from three different sections of a microstructure profile measured in Lake Baikal, and theoretical functions fitted to the spectra. The function has two fit parameters: the dissipation rate ε, which determines the form of the curve, and the rate of diffusive smoothing of temperature, χ, which determines the absolute level of the curve

then converted to spectra by Fourier transformation. The theoretical one-dimensional spectrum

$$\Phi_T = \frac{\chi_T}{2}\sqrt{\frac{D_T}{\gamma^3}}\left[\frac{1}{x}e^{-x^2} - \sqrt{\pi}\,(1 - \mathrm{erf}(x))\right]$$

where $x = k\sqrt{DT/\gamma}$, is finally fitted to the observed spectrum using the two fit parameters χ_T and γ.

4 Wind Set-up, Internal Standing Waves and Modes

Wind set-up Wind blowing in a constant direction over a water body exerts a surface stress $\tau = \rho_{air}\, C_{10}\, U_{10}^2$, which moves the water of the surface layer towards the downwind end. As indicated in Fig. 10 it has two effects on the water body:

- the water level becomes tilted, piling up water on the downwind end and lower the water level on the upwind end, see Fig. 10; and
- the lighter surface layer (epilimnion) becomes deeper on the downwind end, where more surface water is moved to and it becomes thinner on the up-wind end where deep-water is upwelling and replacing surface water, see Fig. 10.

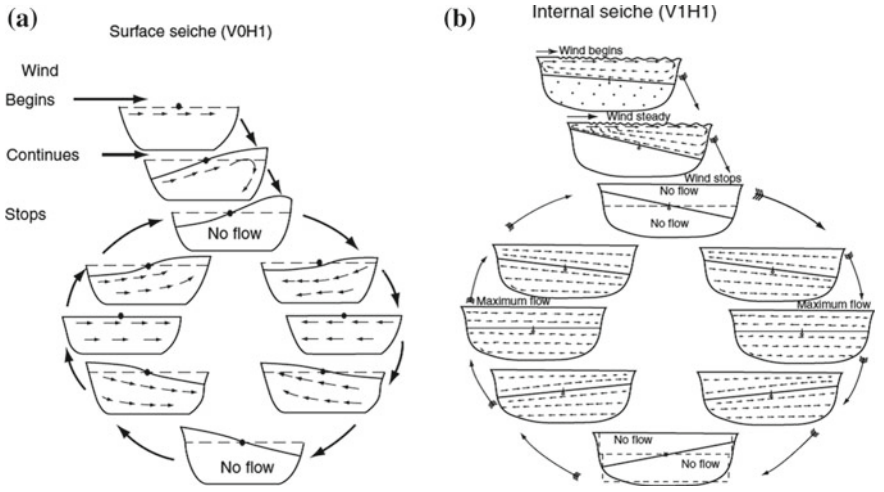

Fig. 10 Movement caused by steady moderate wind stress on a hypothetical layered lake and subsequent internal seiche motion. (*Left*) Horizontal mode-one surface seiche in a homogeneous one-layered system. (*Right*) horizontal-mode one vertical-mode one internal seiche in a two-layered system. The *top* two schemes show the set-up for both modes. The circle below is a schematic of the temporal development of the surface level (*left*) and the pycnocline (*right*) in steps of 1/4 of the seiching period. At 0 and 1/2 period, the energy is purely potential and there is no flow. At 1/4 and 3/4 period, the dislocation is zero and all energy is in kinetic form. Courtesy of Mortimer (1952)

This forcing on stratified lakes leads to internal waves of various temporal and spatial scales. Roughly 20% of the wind energy entering the lake is transferred to large-scale wave motions, called basin-scale internal waves (hereafter BSIW); the remainder being dissipated in the surface layer. These waves temporarily store the wind energy until it is dissipated, mainly by friction along the lake bed. They play a crucial role in the transport of mass and momentum in the lake, driving horizontal dispersion and vertical mixing with great implications for biogeochemical processes and contaminant transport.

Generation of basin scale internal waves To describe the generation of these waves, we start with a simple rectangular lake of length L, width B, and depth H, with a sharp thin thermocline separating a homogenous warm epilimnion of thickness h_1 and density ρ_1 and from a homogeneous cold hypolimnion of thickness h_2 and density ρ_2. A steady wind applied to the lake surface, see Fig. 10, causes an upwelling (setup) of the free-surface and a lowering of the thermocline at the downwind shore. If the wind forcing lasts for more than a quarter of the fundamental mode-one BSIW period (defined below), the thermocline tilt will span the entire basin with a maximum amplitude $\eta_o = Lu_*^2/g'h_1$, where $g' = g(\rho_2 - \rho_1)/\rho_2$ is the reduced gravity as a result of the density difference across the thermocline. The gravitational force acting on the tilted interfacial free-surface and thermocline generates both surface (barotropic) and internal (baroclinic) pressure gradients, which balance the applied wind force. When the wind stops, the gravitational force is unbalanced and the interfaces relax, generating freely propagating basin-scale internal and surface waves, from both upwind and downwind ends of the lake. The upwind and downwind components combine to form basin-scale standing waves on both interfaces, referred to as surface and internal seiches.

A single wind burst or aperiodic wind events lead to free modes with natural periods that depend on the basin shape, the stratification and the Earth's rotation. Conversely, periodic wind forcing (e.g. sea breeze) systematically resets the phase of the wave, leading to forced BSIWs with periods that match those of the wind forcing.

Horizontal pattern of basin scale internal waves A two-layer system is a good approximation for most lakes at mid-latitude during the late summer, see Fig. 11. When the wind relaxes, the oscillation takes the form of a sinusoidal standing wave with antinodes at either end of the basin. The motion is described by the linear shallow water equation, the wave speed $C = \sqrt{g'H_e}$, where $H_e = h_1h_2/(h_1 + h_2)$ the equivalent depth. C depends on the stratification and will change during the season as the thermocline deepens. Different horizontal wave modes can be exited as long as they match the antinodal boundary condition, and the different periods associated with the horizontal modes are $T_n = 2L/nC$, where n is the number of nodes in the horizontal (i.e. the horizontal mode). The first horizontal mode can contain up to 98% of the energy embodied in the initial wind induced thermocline tilt, but basin shape and/or wind forcing can enhance the importance of secondary modes in some cases, see Boegman et al. (2005b).

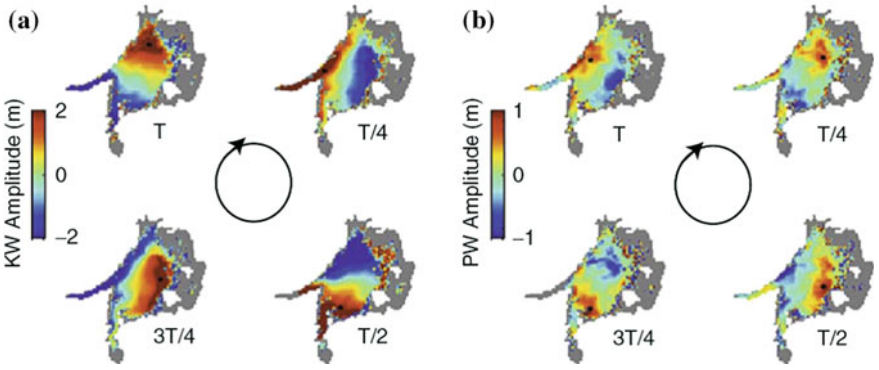

Fig. 11 Example of a Kelvin wave in Lake Simcoe shown as temporal evolution in 1/4 of a period. Evolution of the 15 °C isotherm, representing the thermocline displacement from a three-dimensional hydrodynamic simulation. *Left* Data have been band-pass filtered around the 95-h Kelvin wave period. Each image is offset by a 1/4 of Kelvin wave period (24 h) and shows the counter-clockwise evolution of the wave. *Right* Data have been band-pass filtered around the 14-h Poincaré wave period. Each image is offset by a 1/4 of Poincaré wave period (3.5 h) and shows the clockwise evolution of the wave. The *black dot* in each panel highlights the rotation of the wave crest, and the black *circle* represents the time evolution

Effects of Earth's rotation In large lakes, the Coriolis force, resulting from the Earth's rotation, becomes significant and can modify the wave pattern. The relative importance of the Coriolis force is quantified with the Rossby radius, $R_o = C/f$, and the Burger number, $S = R_o/f$, where $f = \frac{4\pi}{T} \sin\theta$ is the Coriolis parameter, $T = 1$ day, is the period of rotation of the Earth, θ is the latitude and R is a typical length scale characterizing the basin length or width (usually $L/2$). For lakes with $R > R_o$, and $S < 1$ rotational effects are expected. Conversely, in the case $S > 1$, rotational effects can be neglected.

We illustrate the effects of rotation on BSIWs by considering its influence on a longitudinal internal seiche in a large northern hemisphere lake. As the wind-displaced thermocline relaxes, and the seiche begins to propagate across the basin, the Coriolis force pushes the wave toward the right, where it is bounded by the shoreline, causing it to propagate cyclonically (counter-clockwise in the northern hemisphere) along the shore with the wave amplitude decaying exponentially in the offshore direction, see Fig. 11. This wave is called a Kelvin wave, and its period must be greater than the local inertial period, $T_i = 2\pi/f$. The phase velocity and corresponding wave period, T_1, remain the same, for the Kelvin wave, as in the non-rotational case. At a distance of $2R_o$ offshore, the wave is only 10% of its maximum amplitude, so in very large lakes, such as the Laurentian Great Lakes, where $R \gg R_o$, the Kelvin wave is a nearshore phenomenon that takes the form of a coastal jet. In smaller lakes, where $R \sim R_o$, the Kelvin wave signature can be found throughout the basin (e.g. Lake Simcoe, Canada, Fig. 11). We now consider the effect of rotation on the transverse basin-scale internal seiche. Because $L > B$, contrary to the longitudinal seiche, the transverse seiche is not constrained by the boundaries at the longitudinal ends of

the lake. When deflected to the right, by the Coriolis force, the seiche is, therefore, modified into a progressive anticyclonic (clockwise in the northern hemisphere) wave form. Fluid particles displaced by the wave follow anticyclonic circular or elliptical trajectories, known as inertial circles, with radius $r = u/f$, where u is the wave induced current speed. These transverse waves are called inertia-gravity waves or Poincaré waves and the dispersion relation for a rectangular basin, in terms of the wave period, is given by: $1/T_{PW}^2 = 1/T_i^2 + (1 + r^2)/T_1^2$, where $r = B/L$, is the basin aspect ratio at the thermocline depth. The dual character of this wave can be seen in the dispersion relation, where the first term on the right hand side describes the inertial behavior of the inertial circles and the second term has gravitational wave behavior with rectilinear motion. This explains the elliptical pattern of the Poincaré wave with the eccentricity depending on the relative intensity of these two terms. The dispersion relation (above) shows that the Poincaré wave period is typically close but always lower than the inertial period, the shift being a function of the basin shape (through r) and the stratification (through T_1) and can therefore be expressed as a function of S (Antenucci and Imberger (2001)) with the same trend of T_{PW} approaching Ti (inertial wave behavior) as S decreases (i.e., large lake).

Basin scale internal wave damping processes BSIW energy is ultimately damped by dissipation (friction) and the work required by diapycnal mixing. The processes responsible for dissipation and mixing can be linked to external driving factors, such as wind, stratification and basin shape, which energize the waves, using the dimensionless Wedderburn number, W. The magnitude of the wind induced thermocline setup can be quantified according to $W = h_1/\eta_o$, which is the ratio of the restoring baroclinic pressure force (i.e. gravitational force acting on the tilted thermocline) to the applied wind force. In the case of linear BSIWs, $W^{-1} < 0.3$, 90% of the wave energy is dissipated by friction as the seiche induced currents oscillate along the bottom boundary (Imberger (1998); Wüest et al. (2000); Bouffard et al. (2012)). These currents generate a turbulent bottom boundary layer and shear instabilities form where the thermocline oscillates in a swash zone along the lake bed. For $0.3 < W^{-1} < 1.0$, the BSIWs begin to lose energy to smaller-scale nonlinear internal waves, e.g. solitary waves, see Boegman et al. (2005a), which propagate with little energy loss until they shoal and break on sloping topography at the depth of the thermocline; leading to localized dissipation, mixing and sediment resuspension. Under conditions of strong forcing and weak stratification, $W^{-1} > 1.0$, BSIWs will degenerate through the formation of internal hydraulic jumps and/or shear instability in metalimnion of the basin interior. Detailed quantifications of the energy flux paths in lakes can be found in Wüest et al. (2000), Boegman et al. (2005b), Bouffard et al. (2012).

5 Concluding Remarks

Lake and reservoir ecosystems are strongly affected by anthropogenic pressure. A first example is the lake eutrophication and related harmful algae bloom development. A second example is the impact of climate change and related increased stratification strength and duration. Both require good managing strategies to preserve or restore the ecosystem integrity. Efficient guidance for lake and reservoir managers comes with capabilities to evaluate mixing and transport in stratified flows. In the past, many studies have focused on the connection between small-scale turbulence and the large-scale basin-scale internal waves transport. While still an active research field, recent developments of measurement techniques such as satellite observation, autonomous underwater vehicles, automatized profilers have open new horizons and, today, allow to investigate at high frequency the lateral variability in lakes. Yet, the role of mesoscale rotating eddies in the large to small-scale energy transfer remains largely unexplored in lakes and is a promising research topic.

References

J.P. Antenucci, J. Imberger, Energetics of long internal gravity waves in large lakes. Limnol. Oceanogr. **46**(7), 1760–1773 (2001)

L. Boegman, G.N. Ivey, J. Imberger, The degeneration of internal waves in lakes with sloping topography. Limnol. Oceanogr. **50**(5), 1620–1637 (2005a)

L. Boegman, G.N. Ivey, J. Imberger, The energetics of large-scale internal wave degeneration in lakes. J. Fluid Mech. **531**, 159–180 (2005b)

D. Bouffard, L. Boegman, Y.R. Rao, Poincaré wave-induced mixing in a large lake. Limnol. Oceanogr. **57**(4), 1201–1216 (2012)

D. Bouffard, L. Boegman, A diapycnal diffusivity model for stratified environmental flows. Dyn. Atmos. Oceans **61**, 14–34 (2013)

D.R. Caldwell, T.M. Chriss, The viscous sublayer at the sea floor. Science **205**(4411), 1131–1132 (1979)

T.M. Dillon, T.M. Powell, Observations of a surface mixed layer. Deep-Sea Res. Part A Oceanographic Res. Papers, **26**(8), 915–932 (1979)

A.E. Gargett, T.B. Sanford, T.R. Osborn, Surface mixing layers in the Sargasso Sea. J. Phys. Oceanogr. **9**(6), 1090–1111 (1979)

J. Imberger, Flux paths in a stratified lake. Phys. Processes Lakes Oceans **54**, 1–17 (1998)

D.M. Imboden, A. Wüest, Mixing mechanisms in lakes. in *Physics and Chemistry of Lakes*, (Springer, New York , 1995), pp. 83–138

G.N. Ivey, J. Imberger, On the nature of turbulence in a stratified fluid. Part I: The energetics of mixing. J. Phys. Oceanogr. **21**(5), 650–658 (1991)

G.N. Ivey, K.B. Winters, J.R. Koseff, Density stratification, turbulence, but how much mixing? Annu. Rev. Fluid Mech. **40**, 169–184 (2008)

B.B. Jorgensen, D.J. Des Marais, The diffusive boundary layer of sediments: Oxygen microgradients over a microbial mat. Limnol. Oceanogr. **35**(6), 1343–1355 (1990)

I. Langmuir, Surface motion of water induced by wind. Science **87**(2250), 119–123 (1938)

S. Leibovich, The form and dynamics of Langmuir circulation. Annu. Rev. Fluid Mech. **15**, 391–427 (1983)

A. Lorke, L. Umlauf, T. Jonas, A. Wüest, Dynamics of turbulence in low-speed oscillating bottom-boundary layers of stratified basins. Environ. Fluid Mech. **2**(4), 291–313 (2002)
C.H. Mortimer, Water movements in lakes during summer stratification–Evidence from the distribution of temperature in Windermere. Philosophical Trans. R. Soc. London B Biological Sci. **236**(635), 355–398 (1952)
B. Mueller, L.D. Bryant, A. Matzinger, A. Wüest, Hypolimnetic oxygen depletion in eutrophic lakes. Environ. Sci. Technol. **46**(18), 9964–9971 (2012)
A. Wüest, G. Piepke, D.C. van Senden, Turbulent kinetic energy balance as a tool for estimating vertical diffusivity in wind-forced stratified waters. Limnol. Oceanogr. **45**(6), 1388–1400 (2000)
A. Wüest, A. Lorke, Small-scale hydrodynamics in lakes. Annu. Rev. Fluid Mech. **35**, 373–412 (2003)
A. Wüest, A. Lorke, Small-scale turbulence and mixing: Energy fluxes in stratified lakes. Encyclopedia Inland Waters **1**, 628–635 (2009)